Tunable Hybrid Qubit in a Triple Quantum Dot

Bao-Chuan Wang, Gang Cao, Hai-Ou Li, Ming Xiao, Guang-Can Guo, Xuedong Hu, Hong-Wen Jiang, and Guo-Ping Guo

Phys. Rev. Applied **8**, 064035 — Published 29 December 2017

DOI: 10.1103/PhysRevApplied.8.064035

A tunable hybrid qubit in a triple quantum dot

Bao-Chuan Wang,[1, 2] Gang Cao,[1, 2,*] Hai-Ou Li,[1, 2] Ming Xiao,[1, 2] Guang-Can Guo,[1, 2] Xuedong Hu,[3] Hong-Wen Jiang,[4] and Guo-Ping Guo[1, 2,*]

[1] *Key Laboratory of Quantum Information, University of Science and Technology of China, Chinese Academy of Sciences, Hefei 230026, China*

[2] *Synergetic Innovation Center of Quantum Information & Quantum Physics, University of Science and Technology of China, Hefei, Anhui 230026, China*

[3] *Department of Physics, University at Buffalo, SUNY, Buffalo, New York 14260, USA*

[4] *Department of Physics and Astronomy, University of California at Los Angeles, California 90095, USA*

[*]Corresponding Authors: gcao@ustc.edu.cn; gpguo@ustc.edu.cn

Abstract

We experimentally demonstrate quantum coherent dynamics of a triple-dot-based multi-electron hybrid qubit. Pulsed experiments show that this system can be conveniently initialized, controlled, measured electrically, and has good ratio Q ~ 29 between the coherence time and gate time. Furthermore, the current multi-electron hybrid qubit has an operation frequency that is tunable in a wide range, from 2 to about 15 GHz. We have also provide qualitative understandings of the experimental observations by mapping it onto a three-electron system. The demonstration of the high tunability in a triple dot system could be potentially useful for future quantum control.

I. INTRODUCTION

A fully controllable two-level system is an essential building block toward a scalable quantum computer. A gate-defined semiconductor quantum dot (QD), which can be manipulated electrically and fabricated using modern microelectronic technology, is considered an ideal platform for quantum computation [1–3]. Over the past decade, extensive progress has been achieved in the exploration of qubits based on the spin and charge degrees of freedom of QD-confined electrons [4–19]. An important objective in these studies is to improve the number of gate operations within the coherence time. Although spin qubits, which couple weakly to their environments, have long coherence times, their single-qubit operations are relatively slow [6,8,13,14]. In contrast, charge qubits can be manipulated quickly, albeit within a short coherence time, because of the strong electrical interaction [16–19].

A hybrid qubit of charge and spin is a practical scheme which aims to achieve fast operations with a reasonably long coherence time by taking advantage of parallel energy levels. Using a non-adiabatic pulse, x rotation can be realized near a charge transition, while z rotations can be obtained in the region with parallel energy structure, so that dephasing is suppressed efficiently. Two-hybrid-qubit gates can be implemented using electric dipole coupling [20, 21]. Recently, experiments on the hybrid qubit in a Si/SiGe heterostructure have demonstrated fast coherent control using both pulse- and microwave-driven mechanisms [22–24]. By tuning the qubit parameters, Ramsey and Rabi decay times have been extended to more than 120 ns and 1 μs, respectively [25]. However, tunable operation frequency for this qubit design remains a difficult challenge because the qubit energy splitting is based on valley splitting in Si.

Adding quantum dots and/or electrons inevitably increase the size of the system Hilbert space, thus allowing a broader search for an optimal qubit encoding scheme that is both controllable and coherent [26]. For instance, a triple quantum dot with multiple interacting electrons has a highly tunable energy structure. All-exchange qubit based on three electrons in a triplet dot is one such example [27-30]. We have

also studied a tunable hybrid qubit in a five-electron GaAs double quantum dot by taking advantage of the asymmetry-split excited states in one of the dots [31]. In short, increasing the number of electrons and/or quantum dots allows tuning of the mixture between charge and spin degrees of freedom, therefore provides a potential path to realize an optimally encoded qubit.

In this Letter we report an experimental exploration to realize a controllable hybrid qubit in a linear triple quantum dot with asymmetric tunnel couplings in the multi-electron charge configuration of (6,2,3)-(7,1,3). We perform pulsed experiments to generate coherent oscillations that indicate the presence of quasi-parallel energy levels, the same favorable characteristics displayed by the double-dot hybrid qubit [20, 21]. More importantly, we find that the energy splitting of our hybrid qubit can be tuned conveniently in a wide range. By mapping our complex energy structure onto that of a three-electron triple dot, we provide a qualitative description of our experimental observations. The results could potentially lead to various applications, including a new encoding scheme that can be exploited on the triplet dot structure.

II. RESULTS AND DISCUSSIONS

A. Experimental setup

The linear triple dot we study is fabricated on a GaAs/AlGaAs heterostructure using a combination of photolithography and electron beam lithography, as is illustrated by the scanning electron microscopy image shown in Fig. 1(a). The two-dimensional electron gas is located about 90 nm below the surface of the heterostructure. The density and mobility of the two-dimensional electron gas are $2.0 \times 10^{11} cm^{-2}$ and $1.2 \times 10^{5} cm^{2} \cdot V^{-1} \cdot s^{-1}$, respectively. Metal gates (Ti-Au) D1–D7, H1 and H2 form the triple dot array, while gates U1–U3, together with H1 and H2, create a quantum point contact (QPC) as a sensor of the charge states of the quantum dot array. The transconductance response of the QPC channel is acquired using a lock-in amplifier with a small ac modulation voltage (typically 0.2 mV)

applied to gate D1. A high-frequency signal, passing through a semi-rigid coaxial cable from a room-temperature environment, is also applied to gate D1 using a bias tee. The device is cooled inside a dilution refrigerator at a base temperature of 20 mK.

B. Charge stability diagram

A typical charge stability diagram in Fig. 1(b) of our device shows three distinct charging line slopes (indicated by three dashed lines) corresponding to the three quantum dots [32], with the green (blue, black) dashed line indicating the charging line of the left (middle, right) dot. A careful investigation of the charge occupation indicates that the charge transition we study here (marked by the circle) is (6,2,3) to (7,1,3), where (l,m,r) denotes the electron numbers in the left, middle, and right dot, respectively. The smooth (sharp) anti-crossing marked by the rectangle (circle) implies that the middle and right (left) dots have strong (weak) tunnel coupling [33].

Our manipulations are always initialized in the ground state of charge configuration (6,2,3). Figure 1(c) shows the charge stability diagram near the area of the charge transition between (7,1,3) and (6,2,3) for a short pulse duration of t_p = 200 ps and a pulse height of V_p = 400 mV, with a repetition rate of 40 MHz. The region between the two white dashed lines is the area where the pulse can drive the electron non-adiabatically go through the transition line (upper dashed line) between (7,1,3) and (6,2,3). And the coherent oscillations are generated between the two lowest-energy states of the triple dot in (7,1,3) configuration. The fringes, marked by the yellow arrows, indicate Landau-Zener-Stückelberg interference in the (7,1,3) charge configuration, similar to what we observed before in other experiments [15–17].

C. Quasi-parallel energy spectrum

Figure 2(a) shows the transconductance of the QPC channel as a function of the pulse duration time t_p and the detuning ε_p from the starting point of the pulse

[together with pulse height, it would determine how deep the system is pushed into the (7,1,3) region]. Two easily distinguishable patterns are indicated in pink and green in Fig. 2(b). The green-line pattern, corresponding the x-axis rotations, is right at the boundary separating the (7,1,3) and (6,2,3) region. It has the shape of a letter V on the side, and is characteristic of a lock-in measurement of a charge qubit, also known as a charge-qubit Larmor oscillation pattern [17, 23]. We thus conclude that the green pattern here results from charge oscillations between the left and middle dot, i.e. between (7,1,3) and (6,2,3) configurations for the three dots.

The pink-line oscillation pattern, corresponding the z-axis rotations, resides completely within the (7,1,3) region. It has nearly parallel fringes as we vary the detuning point within (7,1,3), indicating that the oscillation frequency depends only weakly on ε_p (which is equivalent to the interdot detuning between the left and the middle dot). To extract the oscillation frequency's dependence on detuning, we perform a fast Fourier transform on the data of Fig. 2(a), and show the result in Fig. 2(c). Clearly, the oscillation frequency changes slowly in a large range of the left-middle detuning. Since the oscillation frequency is given by the energy difference between the two relevant states accessible through the fast-pulse technique, we conclude that the energy splitting varies only slowly with the detuning, indicating a quasi-parallel energy spectrum.

Figure 2(d) is a line cut of the data along the red dashed line in Fig. 2(a), after subtracting a smooth background. A fit in the form $Aexp[-(t-t_0)^2/T_2^{*2}]cos\,(\omega t+\theta)$ gives $T_2^* = 4.0\,ns$, shown by the red solid line in Fig. 2(d). The frequency of the coherent oscillation is ~3.6 GHz, corresponding to a gate-time of ~140 ps. The Q-factor is thus ~29 (the ratio between decoherence and gate-time) which indicates that our qubit has reasonably good quantum coherence. While this dephasing time is much faster than a spin qubit, it is on par with an un-optimized double dot hybrid qubit [23, 25].

We can make two observations from the experimental results obtained here. First, the coherent oscillations cannot be due to a hyperfine field gradient between the dots. The frequency of these oscillations is far too high to be generated by the small

nuclear field. Second, the oscillations cannot be due to charge oscillations between the left and middle dots as in the case of a charge qubit, because the oscillation frequency of a charge qubit should be sensitive to ε_p, and the observed oscillations occur within the (7,1,3) region. We thus conclude with confidence that the coherent oscillations we have observed here are Larmor oscillations between the ground and first excited states within the (7,1,3) region.

D. Tunable oscillation frequency

Further investigation of the triple dot reveals another interesting feature, as shown in Fig. 3. Specifically, we find that the frequency of the coherent oscillation depends sensitively on the gate voltage on D6, which presumably influences the detuning of the right dot the most, while the coherent oscillation seems to occur in the left two dots where charge occupation has changed relative to the initial state. Figure 3(a) to 3(d) presents the measured QPC transconductance response for four different D6 gate voltages. The oscillation frequency changes more than three times, from about 2 to about 7 GHz, as the D6 voltage changes only 15%, from −0.5 to −0.42 V. In Fig. 4(a) we present a more complete dependence of the oscillation frequency on the D6 voltage. The frequency can be continuously increased to ~15 GHz by increasing the D6 voltage, at which point the oscillation is too fast to resolve.

The tunable oscillation frequency indicates that the energy difference between the parallel energy levels depends sensitively on the detuning of the right dot. Superficially this seems counter-intuitive, as the coherent oscillation is generated by changing the charge occupation in the left two dots, with the right dot occupation remaining constant. However, as we discuss in our theoretical model below, this unexpected dependence becomes quite reasonable when we realize that all three dots are coupled, and the relevant states are multi-electron states extended over all three dots.

We have extracted the coherence time of each frequency using data from the line cut at $\varepsilon = -80$ μeV. The results are presented using the blue dots in Fig. 4(a). Clearly, the two quantities display opposite trends: as the coherent oscillation

frequency increases from 2 to 15 GHz, coherence time decreases from 6 to 1 ns.

Summarizing our experimental results, we observed coherent oscillations between the ground and first excited states within the (7,1,3) charge configuration with reasonably good coherent properties, and found that the oscillation frequency depends sensitively on the detuning of the right dot but insensitively on the detuning between the left and middle dot. The important questions we need to answer now are thus, first, what are the two states between which the coherent oscillations occur, and second, why the observed oscillation frequency has the particular detuning dependences.

III. THEORETICAL EXPLANATIONS

A. Theoretical model based on the three outer-shell electrons

A theoretical calculation of the eigenenergies and eigenstates of 11 electrons in a triple dot is not impossible. However, the strong Coulomb interaction and the resulting electron correlations mean that the eigenstates will not be single Slater determinants from single-particle states. Instead the electron eigenstates are always superpositions of multiple Slater deteminants, or "configurations". As such even an analytical solution would hardly give us any intuition on our problem. We thus focus on the qualitative physical picture and do not attempt to obtain a numerically accurate description of our system through a full-scale configuration interaction calculation.

There are two key features for the states of our triple dot, the charge distribution within each dot, and the spin symmetry of the many-electron states involved in our study. The former explains why we cannot repeat our experiments at lower charge occupation numbers. In other words, the electrons occupying the larger excited orbitals also see a lower tunnel barrier, making it much easier for us to observe correlated dynamics in the triple dot. The later feature, on spin symmetry, helps us map our multi-electron system onto a simpler system, and allows us to provide a qualitatively sensible physical picture for our experimental observations. Below we

focus on this mapping.

Since Coulomb interaction is not spin dependent, each of the multi-electron eigenstates has a specific spin symmetry. For example, Hund's Rule dictates that in the ground state, 6 of the 7 electrons in the left dot should pair-up and form spin-singlets in the lowest three orbital states. Since our quantum dots are two-dimensional and nearly circular, these orbitals states should be the S and P Fock-Darwin states. Excitations from these close-shell states requires large energy, thus should contribute less to the low-energy states. Therefore the spin property of the 7 electrons in the right dot is determined by the lone outer-shell electron. The same argument can be made for the three electrons in the right dot. In all, we can thus argue that the spin symmetry of our triple-dot multi-electron states can be mapped to those for three electrons near the (1,1,1)-(0,2,1) charge transition.

To explain the basic features of our observations, we build a simple model based on the three outer-shell electrons (more details can be found in the Appendix). As schematically shown in Fig. 4(b), the qubit can be manipulated similar as the original hybrid qubit. The initial state of our experiment is the ground state in the (0,2,1) configuration with zero applied magnetic field, and the spin state (considering only the $S_z = +1/2$ component, without loss of generality since we do not consider spin-flip tunneling) is $|S\rangle_M|\uparrow\rangle_R$, where the subindex indicates the dot where the electrons are located [20-22]. The system is then driven to the (1,1,1) configuration with interdot exchange couplings J_{LM} and J_{MR} [26, 27]. We can use a spin Hamiltonian here because we have excluded charge dynamics between (1,1,1) and (0,2,1) so that we can focus on the spin dynamics within the (1,1,1) charge configuration.

The key to our observed coherent oscillation is that $J_{LM} \neq J_{MR}$ in our case, such that the total spin S is not a good quantum number (while S_z is). The ground $|g\rangle$ and first excited $|e\rangle$ states are thus mixtures of $|\uparrow\rangle_L|S\rangle_{MR}$ and $\sqrt{1/3}\,|\uparrow\rangle_L|T_0\rangle_{MR} - \sqrt{2/3}\,|\downarrow\rangle_L|T_+\rangle_{MR}$ states [34], or the logical qubit states for the all-exchange qubit architecture [28-30]. In other words, when the system is suddenly driven from the

initial (0,2,1) configuration into (1,1,1), both the ground and first excited states have finite probabilities of being occupied (see Appendix). The frequency of the ensuing coherent Larmor oscillation is at the energy splitting between these two states, given by $\sqrt{J_{LM}^2 + J_{LM}J_{MR} + J_{MR}^2}$.

The expression of the oscillation frequency hints at why we have the observed dependences on the two detunings. Specifically, at the limit when $J_{MR} \gg J_{LM}$, the oscillation frequency is approximately $J_{MR} + J_{LM}/2$, which is mostly determined by J_{MR} and only slightly affected by J_{LM}. In other words, even though our pulse creates a charge transition between the left and middle dots, the frequency of the resulting coherent oscillation in the (1,1,1) regime is actually mostly determined by the stronger coupling between the middle and right dots, which is sensitive to the detuning between the middle and right dots controlled by D6 voltage. Conversely, the detuning between left and middle dots mostly affects J_{LM}, which only influences the oscillation frequency slightly. Thus our results seem insensitive to the left-middle detuning. In short, the tunable operation frequency presented in Fig. 4(b) is expected within this model.

The decrease in dephasing time in Fig. 4(a) can also be interpreted straightforwardly. Specifically, as J_{MR} increases, dephasing of the coherent oscillation becomes increasingly susceptible to fluctuations in J_{MR}, so that decoherence effect of charge noise or other fluctuations becomes dominated by its influence on J_{MR}. Consequently, if we can identify a sweet spot for J_{MR}, it should be possible to have fast oscillations while enjoying good coherence properties [35-37].

Clearly, the addition of a third dot significantly increases the tunability of the qubit splitting compared to the original double-dot hybrid qubit. Different from the all-exchange qubit in which the middle dot symmetrically couples to the neighboring two dots, our qubit works in the asymmetric region without an external magnetic field. Both ground and excited states in our case are coupled to the initial state, so that there is no spin blockade, and the pulse repetition rate we employed is as fast as that of a

charge qubit.

B. Discussions

To compare our simple model with the key experimental observations, let us first summarize the facts. First, coherent oscillations can be observed within the (7,1,3) charge configuration when the triple dot system is prepared in the (6,2,3) configuration. Second, the frequency of the coherent oscillation depends sensitively on the exchange coupling between the middle and the right dot (J_{MR}, or J) but insensitive to the exchange coupling between the middle and the left dot (J_{LM}, or j). Third, the outcome can be measured quickly using a charge sensor as the system is driven back to the (6,2,3) regime.

The coherent oscillation is observed within the (7,1,3) [or effectively, (1,1,1)] charge configuration. Therefore the oscillation cannot correspond to a charge oscillation between dots. Instead it has to be between two states of the same charge configuration that can both be populated by the initial state in the (6,2,3) [effectively (0,2,1)] configuration. Our simple model is consistent with this observation since both $|g\rangle$ and $|e\rangle$ couple to the initial state.

The tunability and charge sensitivity of the coherent oscillation also come out naturally from our simple model, where the oscillation frequency between $|g\rangle$ and $|e\rangle$ is given by $J - j/2 = J_{MR} - J_{LM}/2$ at the lowest order accuracy. The only assumption we need to make here is that $J_{MR} >> J_{LM}$. As long as this approximation holds, the oscillation frequency will have a sensitive dependence on the detuning between the middle and right dot, which determines J_{MR}. Similarly, the change of pulse height ε_p, which determines how far the system is pushed into the (7,1,3) regime, modifies J_{LM}. Since the energy splitting is dominated by J_{MR}, changing J_{LM} would not affect the oscillation frequency significantly. This is thus

consistent with the results presented in Fig.2.

Lastly, our measurement protocol is that for a charge qubit, in the sense that the measurement time is only 30 ns. Therefore the mechanism of measurement cannot be spin blockade. Instead the most likely scenario is the differential tunneling rate between the two (7,1,3) states. In this respect, in our simple model measurement can certainly be accommodated reasonably.

In short, with $J >> j$ we can explain the experimental observations and understand the fast measurement and initialization. We thus believe this model is a reasonable qualitative representation of our experimental study.

IV. CONCLUSIONS

In conclusion, we have demonstrated a tunable hybrid qubit in a triple quantum dot. The coherent oscillations we observe are results of free evolution between two energy levels insensitive to the left-middle detuning, while highly tunable by the right-middle detuning. If a sweet spot can be found for the right-middle exchange coupling, this design has the potential of being widely tunable, highly coherent, and easily controllable. We hope that the results and discussions presented here stimulate further explorations into the quantum coherent dynamics in the few-electron regime for semiconductor quantum processors and nanoelectronics.

Acknowledgements: This work was supported by the National Key R & D Program (Grant No. 2016YFA0301700), the National Natural Science Foundation of China (Grants No. 11674300, No. 61674132, No. 11625419, No. 11575172, and No. 91421303), the “Strategic Priority Research Program (B)” of the Chinese Academy of Sciences (Grant No. XDB01030100), and the Fundamental Research Fund for the Central Universities. X.H. and H.W.J. acknowledge financial support by U.S. Army Research Office through Grants No. W911NF1210609 and No. W911NF1410346, respectively.

APPENDIX: THEORETICAL METHODS

As we discussed in the main text, the qualitative features of many-electron states of the (7,1,3) and (6,2,3) charge configurations are similar to those of the (1,1,1) and (0,2,1) configurations. Since the observed coherent oscillations occur in the (7,1,3) regime, we attempt to understand these oscillations by examine the states of the equivalent (1,1,1) regime.

In the (1,1,1) charge configuration, the spin Hamiltonian for the three electrons is

$$H = J_{MR}\vec{S}_M \cdot \vec{S}_R + J_{LM}\vec{S}_L \cdot \vec{S}_M .$$

When $J_{MR} >> J_{LM}$, we can treat the second part of the Hamiltonian as a perturbation, and start with the eigenstates of the first part of the Hamiltonian. Thus for basis of expansion we use product states of the single-spin eigenstates in the left dot and two-spin eigenstates of the middle and right dots (S_{MR} and T_{MR}). In the $S_z = 1/2$ manifold, these states are:

$$|0\rangle = |\uparrow\rangle_L |S\rangle_{MR} = \frac{1}{\sqrt{2}}|\uparrow\uparrow\downarrow - \uparrow\downarrow\uparrow\rangle$$

$$|1\rangle = \frac{1}{\sqrt{3}}\left[|\uparrow\rangle_L |T_0\rangle_{MR} - \sqrt{2}\,|\downarrow\rangle_L |T_+\rangle_{MR}\right] = \frac{1}{\sqrt{6}}|\uparrow\uparrow\downarrow - 2\downarrow\uparrow\uparrow + \uparrow\downarrow\uparrow\rangle$$

$$|Q\rangle = \frac{1}{\sqrt{3}}\left[\sqrt{2}\,|\uparrow\rangle_L |T_0\rangle_{MR} + |\downarrow\rangle_L |T_+\rangle_{MR}\right] = \frac{1}{\sqrt{3}}|\uparrow\uparrow\downarrow + \downarrow\uparrow\uparrow + \uparrow\downarrow\uparrow\rangle .$$

Since $|0\rangle$ and $|1\rangle$ do not couple to $|Q\rangle$ even when we introduce $J_{LM}\vec{S}_L \cdot \vec{S}_M$ coupling, we can focus on $|0\rangle$ and $|1\rangle$.

The total spin Hamiltonian in the (1,1,1) charge configuration is:

$$\begin{aligned} H &= J_{MR}\vec{S}_M \cdot \vec{S}_R + J_{LM}\vec{S}_L \cdot \vec{S}_M \\ &= \frac{J}{4}\vec{\sigma}_M \cdot \vec{\sigma}_R + \frac{j}{4}\vec{\sigma}_M \cdot \vec{\sigma}_L \\ &= H_0 + \delta H. \end{aligned}$$

Notice we have replaced J_{MR} by J and J_{LM} by j for a more concise notation.

Here H_0 have eigenstates $|0\rangle$ and $|1\rangle$ with energies of $-\frac{3}{4}J$ and $\frac{J}{4}$ respectively. On the other hand, $\langle 0|\delta H|0\rangle = 0$, $\langle 1|\delta H|1\rangle = -\frac{j}{2}$ and $\langle 0|\delta H|1\rangle = \frac{\sqrt{3}}{4}j$. Thus we can write the Hamiltonian as:

$$H = H_0 + \delta H = \begin{pmatrix} -\frac{3}{4}J & \frac{\sqrt{3}}{4}j \\ \frac{\sqrt{3}}{4}j & \frac{3}{4}J - \frac{1}{2}j \end{pmatrix}.$$

The resulting eigenenergies of the H are:

$$\lambda = \frac{1}{2}\left[-\frac{1}{2}(J+j) \pm \sqrt{J^2 - J\cdot j + j^2}\right] = \frac{1}{2}\left[-\frac{1}{2}(J+j) \pm J\sqrt{1 - \frac{j}{J} + \left(\frac{j}{J}\right)^2}\right].$$

Since $J >> j$, using Taylor expansion, the eigenenergies can be written as:

$$\lambda = \frac{1}{2}\left[-\frac{1}{2}(J+j) \pm \left(J - \frac{1}{2}j + \frac{3}{4}\frac{j^2}{J}\right)\right],$$

and the eigenstates of the total Hamiltonian in the (1,1,1) regime are: $|g\rangle = \alpha|0\rangle + \beta|1\rangle$ and $|e\rangle = -\beta|0\rangle + \alpha|1\rangle$ with $\beta = -\sqrt{3}\frac{j}{J}\alpha$. The energy difference between the two eigenstates, at the lowest order, is given by $J - \frac{1}{2}j$.

The initial state in the (0,2,1) regime is $|i\rangle = |S\rangle_M |\uparrow\rangle_R$ assuming that the middle-right-dot coupling is relatively small compared to the exchange spitting within the middle dot. When the voltage pulse is applied, it projects the initial state $|i\rangle$ to $|g\rangle$ and $|e\rangle$ in the (1,1,1) regime through tunneling. Neglecting possible spin flips during the tunneling process, and keeping only the lowest-order single-electron tunneling, we can establish how the initial state is projected into the new eigenstates by examining the branching ratio. The matrix elements of single-particle Hamiltonian between $|i\rangle = |S\rangle_M |\uparrow\rangle_R$, which is in the (0,2,1) charge configuration,

and $|0\rangle$ and $|1\rangle$, which are in the (1,1,1) configuration, are

$$\langle 0|H|i\rangle = -\frac{1}{\sqrt{2}}\left[t_{LM} + \left(\varepsilon_{M\downarrow} + \varepsilon_{R\uparrow}\right)S_{LM}\right]$$

$$\langle 1|H|i\rangle = \sqrt{\frac{3}{2}}\left[t_{LM} + \left(\varepsilon_{M\downarrow} + \varepsilon_{R\uparrow}\right)S_{LM}\right]$$

where t_{LM} is the single-electron tunnel coupling between the ground orbital states of the left and middle dot, S_{LM} is the single-electron wave function overlap between the ground orbital states of the left and middle dots, and $\varepsilon_{M\downarrow}$ and $\varepsilon_{R\uparrow}$ are the single-electron energies of the ground orbitals with different spins in the middle and right dot, respectively. The tunneling matrix elements above indicate that there is a branching ratio of $-\sqrt{3}$ between $|1\rangle$ and $|0\rangle$. In other words, starting from the initial state $|i\rangle$, one electron tunnels from the middle to the left dot, so that the three-electron state becomes:

$$|i\rangle \Rightarrow -\frac{1}{2}|0\rangle + \frac{\sqrt{3}}{2}|1\rangle$$

In the basis of $|g\rangle$ and $|e\rangle$, the three-electron state becomes:

$$|i\rangle \Rightarrow \left(-\frac{\alpha}{2} + \frac{\sqrt{3}}{2}\beta\right)|g\rangle + \left(\frac{\beta}{2} + \frac{\sqrt{3}}{2}\alpha\right)|e\rangle.$$

Denoting the energy splitting between the system excited state $|e\rangle$ and the ground state $|g\rangle$ by $\hbar\omega$, during the evolution in the (1,1,1) regime the spin wave function can be written as:

$$|\psi(t)\rangle = \left(-\frac{\alpha}{2} + \frac{\sqrt{3}}{2}\beta\right)|g\rangle + e^{i\omega t}\left(\frac{\beta}{2} + \frac{\sqrt{3}}{2}\alpha\right)|e\rangle.$$

Here ωt indicates the accumulated phase between $|g\rangle$ and $|e\rangle$ during the pulse. At the end of the pulse, the system shifts back to the (0,2,1) regime, and $|\psi(t)\rangle$ is projected back to $|i\rangle$:

$$|\psi(t)\rangle \Rightarrow \left\{\left(-\frac{\alpha}{2}+\frac{\sqrt{3}}{2}\beta\right)^2 + e^{i\omega t}\left(\frac{\beta}{2}+\frac{\sqrt{3}}{2}\alpha\right)^2\right\}|i\rangle .$$

Since $\beta << \alpha$, we can make our estimate at the limit $\beta \approx 0$, $\alpha \approx 1$ for the probability to find the system in the initial state $|i\rangle$, which is the ground state in the (0,2,1) regime, as:

$$p_i = \frac{5}{8}+\frac{3}{8}\cos(\omega t).$$

This indicates that the return probability is between 1 and $\frac{1}{4}$.

We note that both $|g\rangle$ and $|e\rangle$ couple to the initial state $|i\rangle$, so that there is no spin blockade. Instead, the two states have different overlap with $|i\rangle$, thus have different rates of returning to $|i\rangle$. This difference in returning rates causes the system to stay in the (7,1,3) charge configuration with duration. In other words, the system spends different average time in (6,2,3) relative to (7,1,3), which causes a change in the average QPC signal.

References

[1] D. Loss and D. P. DiVincenzo, Quantum computation with quantum dots, Phys. Rev. A 57, 120 (1998).

[2] G. Burkard, D. Loss, and D. P. DiVincenzo, Coupled quantum dots as quantum gates, Phys. Rev. B 59, 2070 (1999).

[3] I. Buluta, S. Ashhab and F. Nori, Natural and artificial atoms for quantum computation, Rep. Prog. Phys. 74, 104401 (2011).

[4] T. Hayashi, T. Fujisawa, H. D. Cheong, Y. H. Jeong, and Y. Hirayama, Coherent manipulation of electronic states in a double quantum dot, Phys. Rev. Lett. 91, 226804 (2003).

[5] J. R. Petta, A. C. Johnson, C. M. Marcus, M. P. Hanson, and A. C. Gossard, Manipulation of a single charge in a double quantum dot, Phys. Rev. Lett. 93, 186802 (2004).

[6] J. R. Petta, A. C. Johnson, J. M. Taylor, E. A. Laird, A. Yacoby, M. D. Lukin, C. M. Marcus, M. P. Hanson, and A. C. Gossard, Coherent manipulation of coupled electron spins in semiconductor quantum dots, Science 309, 2180 (2005).

[7] R. Hanson, L. P. Kouwenhoven, J. R. Petta, S. Tarucha, and L. M. K. Vandersypen, Spins in few-electron quantum dots, Rev. Mod. Phys. 79, 1217 (2007).

[8] K. C. Nowack, F. H. L. Koppens, Y. V. Nazarov, and L. M. K. Vandersypen, Coherent control of a single electron spin with electric fields, Science 318, 1430 (2007).

[9] M. D. Shulman, O. E. Dial, S. P. Harvey, H. Bluhm, V. Umansky, and A. Yacoby, Demonstration of entanglement of electrostatically coupled singlet-triplet qubits, Science 336, 202 (2012).

[10] X. Hao, R. Ruskov, M. Xiao, C. Tahan, and H. Jiang, Electron spin resonance and spin–valley physics in a silicon double quantum dot, Nat. Commun. 5, 3860 (2014).

[11] R. Brunner, Y. S. Shin, T. Obata, M. Pioro-Ladrière, T. Kubo, K. Yoshida, T.

Taniyama, Y. Tokura, and S. Tarucha, Two-qubit gate of combined single-spin rotation and interdot spin exchange in a double quantum dot, Phys. Rev. Lett. 107, 146801 (2011).

[12] F. H. L. Koppens, C. Buizert, K. J. Tielrooij, I. T. Vink, K. C. Nowack, T. Meunier, L. P. Kouwenhoven, and L. M. K. Vandersypen, Driven coherent oscillations of a single electron spin in a quantum dot, Nature 442, 766 (2006).

[13] B. M. Maune, M. G. Borselli, B. Huang, T. D. Ladd, P. W. Deelman, K. S. Holabird, A. A. Kiselev, I. Alvarado-Rodriguez, R. S. Ross, A. E. Schmitz, M. Sokolich, C. A. Watson, M. F. Gyure, and A. T. Hunter, Coherent singlet-triplet oscillations in a silicon-based double quantum dot, Nature 481, 344 (2012).

[14] M. Veldhorst, J. C. C. Hwang, C. H. Yang, A. W. Leenstra, B. de Ronde, J. P. Dehollain, J. T. Muhonen, F. E. Hudson, K. M. Itoh, MorelloA, and A. S. Dzurak, An addressable quantum dot qubit with fault-tolerant control-fidelity, Nat. Nano. 9, 981 (2014).

[15] K. D. Petersson, J. R. Petta, H. Lu, and A. C. Gossard, Quantum coherence in a one-electron semiconductor charge qubit, Phys. Rev. Lett. 105, 246804 (2010).

[16] G. Cao, H. O. Li, T. Tu, L. Wang, C. Zhou, M. Xiao, G. C. Guo, H. W. Jiang, and G.-P. Guo, Ultrafast universal quantum control of a quantum-dot charge qubit using Landau–Zener–Stückelberg interference, Nat. Commun. 4, 1401 (2013).

[17] Z. Shi, C. B. Simmons, D. R. Ward, J. R. Prance, R. T. Mohr, T. S. Koh, J. K. Gamble, X. Wu, D. E. Savage, M. G. Lagally, M. Friesen, S. N. Coppersmith, and M. A. Eriksson, Coherent quantum oscillations and echo measurements of a Si charge qubit, Phys. Rev. B 88, 075416 (2013).

[18] H.O. Li, G. Cao, G. D. Yu, M. Xiao, G. C. Guo, H. W. Jiang, and G. P. Guo, Conditional rotation of two strongly coupled semiconductor charge qubits, Nat. Commun. 6, 7681 (2015).

[19] D. Kim, D. R. Ward, C. B. Simmons, J. K. Gamble, R. B. Kohout, E. Nielsen, D. E. Savage, M. G. Lagally, M. Friesen, S. N. Coppersmith, and M. A. Eriksson, Microwave-driven coherent operation of a semiconductor quantum dot charge qubit, Nat. Nano. 10, 243 (2015).

[20] T. S. Koh, J. K. Gamble, M. Friesen, M. A. Eriksson, and S. N. Coppersmith, Pulse-gated quantum-dot hybrid qubit, Phys. Rev. Lett. 109, 250503 (2012).

[21] Z. Shi, C. B. Simmons, J. R. Prance, J. K. Gamble, T. S. Koh, Y.-P. Shim, X. Hu, D. E. Savage, M. G. Lagally, M. A. Eriksson, M. Friesen, and S. N. Coppersmith, Fast hybrid silicon double-quantum-dot qubit, Phys. Rev. Lett. 108, 140503 (2012).

[22] D. Kim, Z. Shi, C. B. Simmons, D. R. Ward, J. R. Prance, T. S. Koh, J. K. Gamble, D. E. Savage, M. G. Lagally, M. Friesen, S. N. Coppersmith, and M. A. Eriksson, Quantum control and process tomography of a semiconductor quantum dot hybrid qubit, Nature 511, 70 (2014).

[23] Z. Shi, C. B. Simmons, D. R. Ward, J. R. Prance, X. Wu, T. S. Koh, J. K. Gamble, D. E. Savage, M. G. Lagally, M. Friesen, S. N. Coppersmith, and M. A. Eriksson, Fast coherent manipulation of three-electron states in a double quantum dot, Nat. Commun. 5, 3020 (2014).

[24] D. Kim, D. R. Ward, C. B. Simmons, D. E. Savage, M. G. Lagally, M. Friesen, S. N. Coppersmith, and M. A. Eriksson, High-fidelity resonant gating of a silicon-based quantum dot hybrid qubit, Npj Quantum Information 1, 15004 (2015).

[25] B. Thorgrimsson, D. Kim, Y. C. Yang, L. W. Smith, C. B. Simmons, D. R. Ward, R. H. Foote, J. Corrigan, D. E. Savage, M. G. Lagally, M. Friesen, S. N. Coppersmith, and M. A. Eriksson, Extending the coherence of a quantum dot hybrid qubit, Npj Quantum Information 3, 32 (2017).

[26] M. Russ and G. Burkard, Three-electron spin qubits, Journal of Physics: Condensed Matter 29, 393001 (2017).

[27] E. A. Laird, J. M. Taylor, D. P. DiVincenzo, C. M. Marcus, M. P. Hanson, and A. C. Gossard, Coherent spin manipulation in an exchange-only qubit, Phys. Rev. B 82, 075403 (2010).

[28] J. Medford, J. Beil, J. M. Taylor, E. I. Rashba, H. Lu, A. C. Gossard, and C. M. Marcus, Quantum-dot-based resonant exchange qubit, Phys. Rev. Lett. 111, 050501 (2013).

[29] J. Medford, J. Beil, J. M. Taylor, S. D. Bartlett, A. C. Doherty, E. I. Rashba, D. P. DiVincenzo, H. Lu, A. C. Gossard, and C. M. Marcus, Self-consistent

measurement and state tomography of an exchange-only spin qubit, Nat. Nano. 8, 654 (2013).

[30] N. Rohling and G. Burkard, Optimizing electrically controlled echo sequences for the exchange-only qubit, Phys. Rev. B 93, 205434 (2016).

[31] G. Cao, H. O. Li, G. D. Yu, B. C. Wang, B. B. Chen, X. X. Song, M. Xiao, G. C. Guo, H. W. Jiang, X. Hu, and G. P. Guo, Tunable hybrid qubit in a GaAs double quantum dot, Phys. Rev. Lett. 116, 086801 (2016).

[32] L. Gaudreau, S. A. Studenikin, A. S. Sachrajda, P. Zawadzki, A. Kam, J. Lapointe, M. Korkusinski, and P. Hawrylak, Stability diagram of a few-electron triple dot, Phys. Rev. Lett. 97, 036807 (2006).

[33] W. G. van der Wiel, S. De Franceschi, J. M. Elzerman, T. Fujisawa, S. Tarucha, and L. P. Kouwenhoven, Electron transport through double quantum dots, Rev. Mod. Phys. 75, 1 (2002).

[34] Y. P. Shim and C. Tahan, Charge-noise-insensitive gate operations for always-on, exchange-only qubits, Phys. Rev. B 93, 121410 (2016).

[35] M. D. Reed, B. M. Maune, R. W. Andrews, M. G. Borselli, K. Eng, M. P. Jura, A. A. Kiselev, T. D. Ladd, S. T. Merkel, I. Milosavljevic, E. J. Pritchett, M. T. Rakher, R. S. Ross, A. E. Schmitz, A. Smith, J. A. Wright, M. F. Gyure, and A. T. Hunter, Reduced sensitivity to charge noise in semiconductor spin qubits via symmetric operation, Phys. Rev. Lett. 116, 110402 (2016).

[36] F. Martins, F. K. Malinowski, P. D. Nissen, E. Barnes, S. Fallahi, G. C. Gardner, M. J. Manfra, C. M. Marcus, and F. Kuemmeth, Noise suppression using symmetric exchange gates in spin qubits, Phys. Rev. Lett. 116, 116801 (2016).

[37] X. C. Yang, and X. Wang, Suppression of charge noise using barrier control of a singlet-triplet qubit, Phys. Rev. A 96, 012318 (2017).

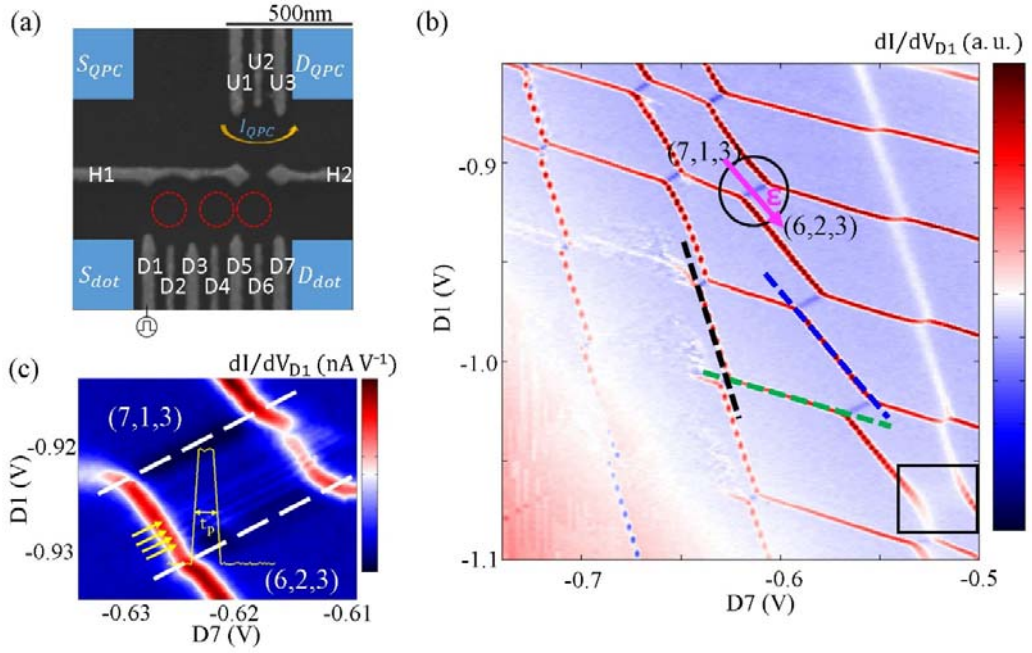

Fig. 1 (a) Scanning electron microscopy image of the device structure, where red dashed circles indicate the approximate quantum-dot positions. (b) Charge stability diagram of the triple quantum dot. Three dashed lines indicate three charging lines with different slopes. The solid circle indicates the area in which we perform our experiment. The pink arrow indicates the detuning direction. (c) Anti-crossing area indicated by the solid circle in (b), after applying a repeated pulse sequence. The inset schematically depicts the pulse sequence in the experiment.

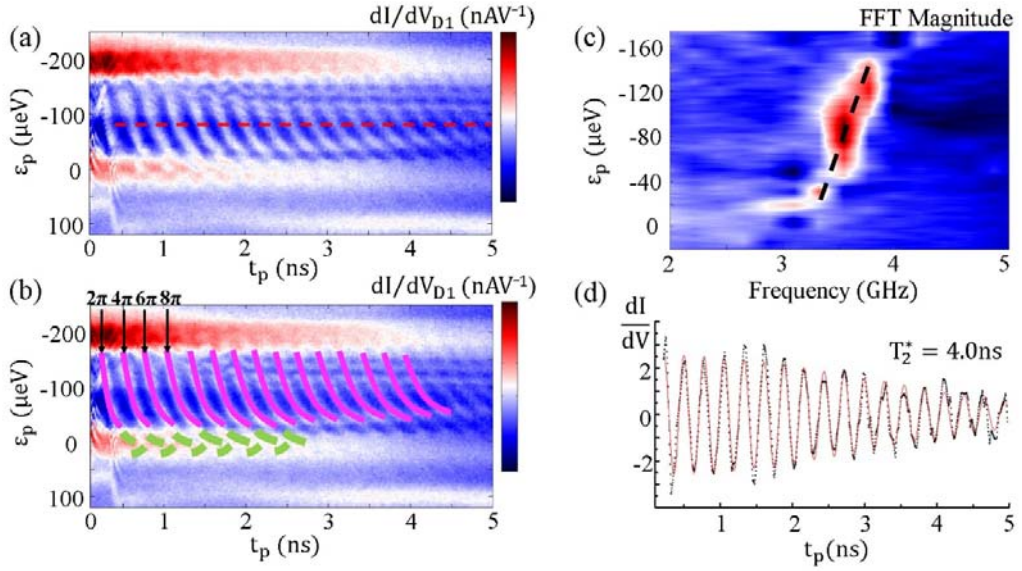

Fig. 2 (a) Coherent charge oscillations as a function of detuning ε_p and pulse duration time t_p. (b) Two highlighted oscillation patterns for clarity of the same data in (a) using pink and green lines. The inserted arrows indicated as 2πN indicate the accumulated total phase. (c) Fast Fourier transform of the data in (a). The dashed guideline indicates frequency variations. (d) Results for the dashed line in (a), after subtraction of a smooth background. The red solid line is a numerical fit, which yields T_2^* = 4.0 ns.

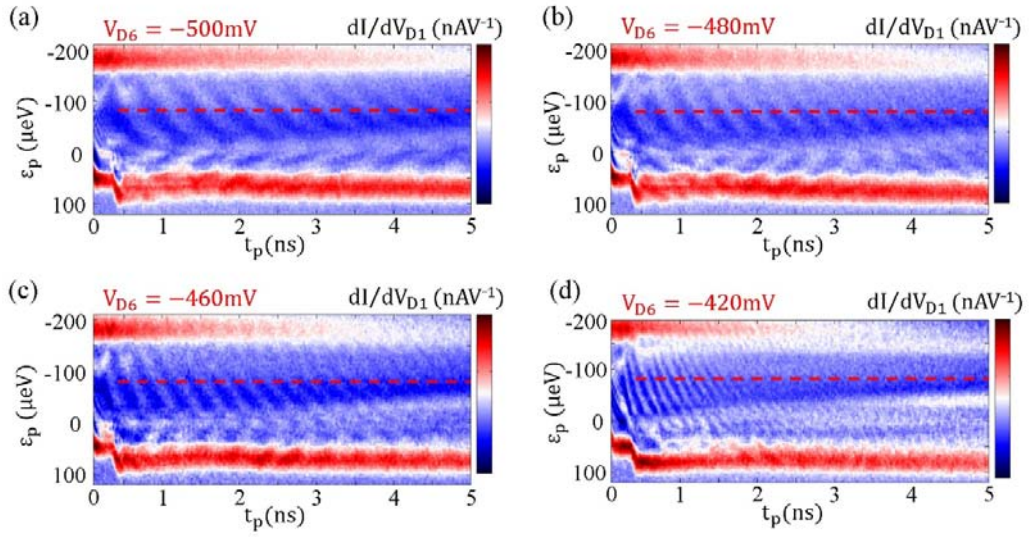

Fig. 3 Coherent charge oscillations as a function of detuning ε_p and pulse duration time t_p for four different values of V_{D6}. The oscillation frequency clearly increases with increasingly positive V_{D6}.

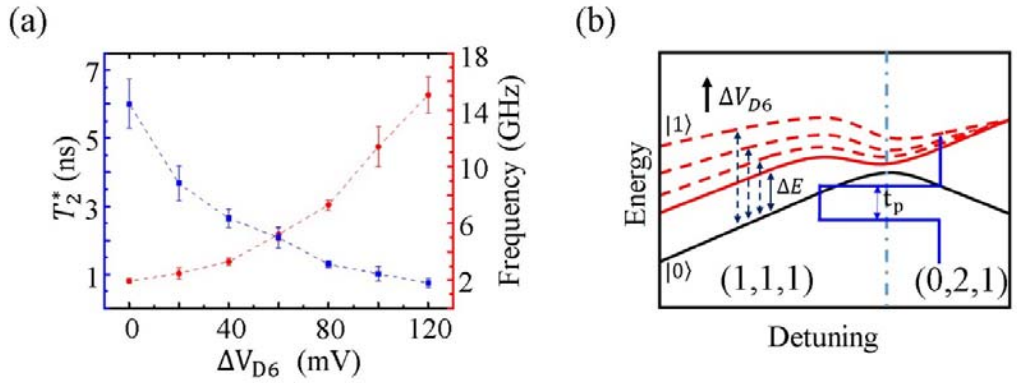

Fig. 4 (a) Charge oscillation frequency and decoherence time as a function of V_{D6}, extracted from the data of red dashed lines in Fig. 3. (b) Schematic diagram of the energy levels variation when changing V_{D6}.